

# Polyhedral Surface: Self-supervised Point Cloud Reconstruction Based on Polyhedral Surface

Hui Tian<sup>1</sup> Kai Xu<sup>1</sup>✉

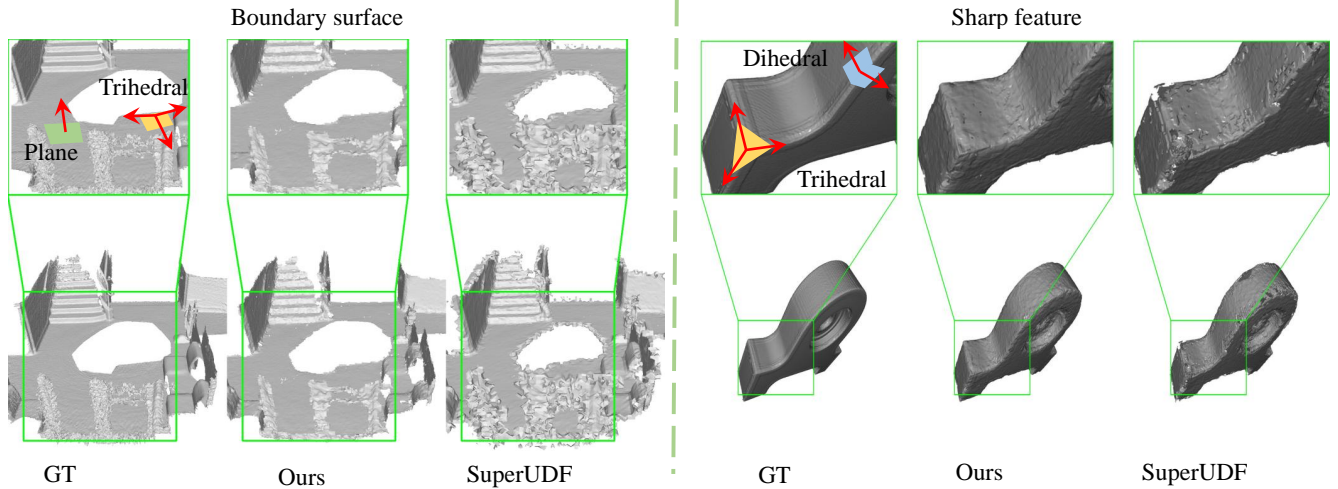


Fig. 1: Polyhedral surface often appears in scenes or shapes. The examples separately show the priority of the polyhedral surface in representing the surface boundary and sharp surface. SuperUDF[1] only makes use of the local geometry plane while ours makes use of the local geometry Polyhedra surface.

**Abstract**—Point cloud reconstruction from raw point cloud has been an important topic in computer graphics for decades, especially due to its high demand in modeling and rendering applications. An important way to solve this problem is establishing a local geometry to fit the local curve. However, previous methods build either a local plane or polynomial curve. Local plane brings the loss of sharp feature and the boundary artefacts on open surface. Polynomial curve is hard to combine with neural network due to the local coordinate consistent problem. To address this, we propose a novel polyhedral surface to represent local surface. This method provides more flexible to represent sharp feature and surface boundary on open surface. It does not require any local coordinate system, which is important when introducing neural networks. Specifically, we use normals to construct the polyhedral surface, including both dihedral and trihedral surfaces using 2 and 3 normals, respectively. Our method achieves state-of-the-art results on three commonly used datasets (ShapeNetCore, ABC, and ScanNet). Code will be released upon acceptance.

**Index Terms**—Polyhedral surface, Point Cloud Reconstruction, Implicit Surface.

## I. INTRODUCTION

Point cloud reconstruction create surface from a set of points in space. This process has numerous applications, including object recognition, scene understanding, and autonomous navigation, and is widely used in fields such as robotics, computer graphics, and virtual reality. With advancements in 3D scanning technologies, point cloud reconstruction has become an increasingly important tool for capturing and modeling

complex real-world scenes. This technique involves gathering data points from a physical object or environment, which are then processed to generate a virtual representation of the object or scene. The resulting 3D model can be used for a variety of purposes, from visualizing complex structures to aiding in the design of new products.

Recent works [2], [3], [4], [5], [6], [7], [8], [9], devote much effort to represent surface in an implicit way. There are two main ways to implicitly represent surface: SDF and UDF. SDF-based method uses a signed distance function to reconstruct a mesh from a distance field, while the UDF-based method uses an unsigned distance function. The SDF-based method is convenient for reconstructing mesh due to its sign existence, but it cannot represent open surfaces. On the other hand, the UDF-based method is good at representing open surfaces, but it has difficulty in establishing smooth mesh due to its discontinuity of gradient near the surface. Because UDF can represent both close and open surface, we choose UDF to represent implicit surface and combine it with polyhedral surface.

There are two common approaches to predict the unsigned distance function (UDF) for point cloud reconstruction. One approach is to use a neural network directly predicting the UDF based on local features, usually via MLP. However, a simple direct prediction of the distance field or occupancy of each query point is usually challenging and hard to handle. Another approach is to build a local geometry model, such as a plane [1] or polynomial curve, and calculate the distance

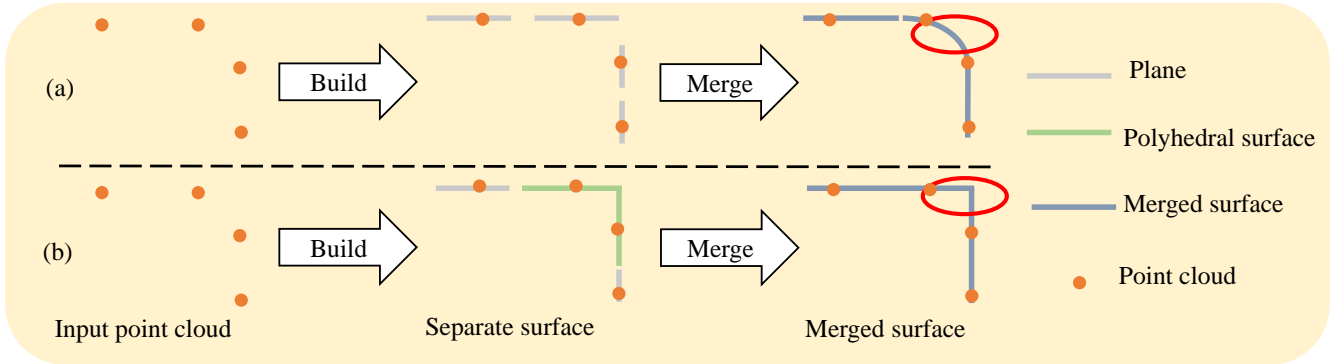


Fig. 2: The advantage of polyhedral surface illustrated in 2D cases. (a) is situation where there is only plane. (b) is the situation where there are plane and polyhedral surface. From the mesh of red circle, the mesh represented by polyhedral surface is close to the GT.

to the surface. However, no one method build a explicit polynomial curve combining with neural network. The reason is local coordinate consistency problem. In traditional method, it is not difficult to build a local coordinate system for local point set. However, when introducing neural networks, each local coordinate system must be consistent with each other, otherwise neural network do not know the local coordinate system and the predicted polynomial parameter is meaningless. It is very hard to build a globally consistent coordinate system. DeepMLS [10] try to solve this problem by combining neural networks with moving least squares using an implicit approach. Instead of representing local geometry with polynomial surface in a 3D coordinate system, deepMLS uses a local plane and merges neighboring planes. This approach avoids the need to establish a local coordinate system but may result in a loss of sharp features, as shown in Fig. 2.

To better represent open surface boundary and sharp local geometry and avoid establishing local coordinate system, we propose the use of polyhedral surfaces instead of local polynomial surface. The polyhedral surface approach allows us to capture intricate details, avoiding the issue of global consistency. Moreover, by integrating polyhedral surface representation with neural networks, we can eliminate the error on the boundary of open surface. Let's delve into the details. In CAD models, open surface boundary and sharp features such as turning surfaces or corners are commonly observed (as depicted in Fig. 1). These features can be naturally represented using polyhedral surfaces. We have designed two types of polyhedral surfaces: dihedral surfaces and trihedral surfaces (as shown in Fig. 1). For the representation of turning surfaces, dihedral surfaces is appropriate. This involves using two normals emitted from the same point to capture the local geometry. The line perpendicular to these two normals represents the intersection line of two planes. Each normal defines a half plane, and the dihedral surface is composed of these two half planes. As the two normals vary, the dihedral surface adapts accordingly. To represent the corners of a cube or open surface boundary, we utilize trihedral surfaces. Here, three normals are employed to capture the local geometry, with each normal corresponding to an edge of the local cube corner. As the normals vary, the trihedral surface adjusts accordingly.

polyhedral surface has the following two advantages with the cost of a little more computation complexity. Firstly, polyhedral surfaces provide a richer local descriptor compared to planes, enabling us to obtain more accurate local geometry. Secondly, we eliminate the need for a global consistent local coordinate system, allowing us to leverage neural networks for prediction of local geometry parameter. Overall, our proposed polyhedral surface method offers a novel and effective way to represent open surface boundary and sharp local geometry, enhancing the accuracy and efficiency of point cloud reconstruction.

In summary, our work makes the following contributions to the field of point cloud reconstruction:

- First, we introduce a novel approach to represent local surfaces by proposing the concept of "polyhedral surfaces", including dihedral and trihedral surface representations. These representations effectively capture the intricate details of local surfaces, providing a more accurate and comprehensive representation, and do not need local coordinate system.
- Second, our method achieves comparable results with state-of-the-art techniques in surface reconstruction from point clouds. By leveraging the advantages of polyhedral surfaces and optimizing the local loss function, we are able to obtain high-quality reconstructions that are on par with the best-performing methods in the field.

These contributions advance the state of the art in point cloud reconstruction and pave the way for further advancements in this important research area.

## II. RELATED WORK

*a) Implicit Method:* Implicit methods, which are mostly deep methods [2], [11], [12], [13], [14], have gained significant attention in the field of point cloud surface reconstruction. With the advancements in deep learning, researchers have focused on leveraging the strong representation ability of neural networks to build better surfaces from point clouds. Neural networks, being able to theoretically fit any function, have been utilized in various ways to learn the distance function or occupancy value of shapes.

One popular approach, DeepSDF [2], encodes the entire shape as a coding and then decodes the signed distance function (SDF) of any query point based on the coding and its position. Occupancy Networks [11], on the other hand, predict only the occupancy value of query points, disregarding distance prediction. It extracts features from the point cloud and uses these features along with position to predict the occupancy value. Convolutional Occupancy Network [12] builds upon Occupancy Networks [11] by integrating 3D convolution into the feature learning process and applying interpolation to obtain the feature of the query point.

Points2Surf [15] aims to regress the absolute SDF value based on local information and classify the sign based on global information. POCO [14] preserves the features of the input point cloud and incorporates a learning-based interpolation module to achieve high-performance reconstruction. NDF [16] introduces the concept of unsigned distance function to represent open surfaces. Neural Pull [17] represents a 3D shape using a single network model and trains the network by predicting the shift of query points.

On-surface Prior [18] adds a geometry prior to Neural Pull, enforcing that the norm of the query point shift to the surface should be minimal. CAP [3] extends the SDF representation of Neural Pull to unsigned distance functions (UDF) and achieves impressive performance. Dynamic Code [19] proposes combining local code with local position encoding to optimize the position of the code. MeshUDF[20] tries to extract mesh directly from the UDF.

From a network design perspective, these methods can be categorized into global methods (e.g., DeepSDF), local methods (e.g., Occupancy Networks, Convolutional Occupancy Network, POCO), and their combinations (e.g., Points2Surf). From the representation method standpoint, these methods can be divided into SDF-based methods (e.g., DeepSDF, Occupancy Networks, Convolutional Occupancy Network, Points2Surf, POCO, Neural Pull, Dynamic Code) and UDF-based methods (e.g., NDF, On-surface Prior, CAP).

*b) Explicit Method:* Explicit methods, such as mesh-based methods, spline functions, and moving least squares (MLS) [21], have been extensively studied in surface reconstruction for several decades. These methods involve constructing a local geometric model, such as a plane, curve, or geometric primitive, to fit the local surface. In our work, we focus on the moving least squares (MLS) family of methods, which includes several relevant approaches that we will discuss in detail.

Moving least squares (MLS) is a popular explicit method that establishes a local coordinate system for each patch and fits a curve based on the local patch information. Implicit moving least squares (IMLS) [22] is an algebraic method that simplifies the local geometry by approximating the curve with a plane. It then merges the local planes using adaptive weights. Robust moving least squares (RMLS) [23] extends MLS by establishing the neighborhood using a forward-search paradigm, enabling it to handle noisy input and capture sharp features.

However, these explicit methods often struggle to leverage the capabilities of neural networks to improve surface recon-

struction. They rely on predefined geometric models and may not effectively capture complex or irregular surfaces.

*c) Combination of Implicit and Explicit Method:* DeepMLS [10] is a successful demonstration of the fusion of explicit and neural network-based methods, building upon the Implicit Moving Least Squares (IMLS) [22] technique. The DeepMLS approach initiates by utilizing a neural network to predict the parameters of local planes. These local planes are subsequently merged using an adaptive weight scheme, resulting in an implicitly represented surface through the calculation of the Signed Distance Function (SDF). While DeepMLS capitalizes on the explicit IMLS method to facilitate the calculation, our work further combines the implicit and explicit methods. It is crucial to discuss these divergent approaches. The implicit method can be readily integrated with neural networks, but it may sacrifice the geometric prior information. Conversely, explicit methods necessitate specific designs to synergize with neural networks, and the flexibility of the geometric prior can be restricted in certain scenarios. In our research, our objective is to enhance the flexibility of the geometric prior compared to the baseline methods, IMLS [22] and DeepMLS [10]. By amalgamating components from both implicit and explicit methods, we strive to devise a novel approach that leverages the strengths of each approach while mitigating their respective limitations.

### III. METHOD

In this section, we present an approach of local surface representation for point cloud reconstruction, referred to as polyhedral surface. Fig. 3 provides an overview of our proposed pipeline. Firstly, we outline the problem and introduce the pipeline. Secondly, we describe the polyhedral surface representation and the methodology for computing the distance from the query point to the polyhedral surface. Thirdly, we discuss the selection of the local surface representation and the merging process for these representations. Fourthly, we elaborate on the refinement method. Lastly, we address the training loss in our approach.

#### A. main pipeline

*a) Formalization:* First, we will formalize our method. We define the space as  $\mathcal{S} = [-1, 1]^3$ . Given an input point cloud  $\mathcal{P} = \{p_1, p_2, \dots, p_n, p_i \in \mathcal{S}\}$ , our objective is to learn a function represented by a neural network  $s(q) = \mathcal{F}(\mathcal{P}, q)$ , where  $q \in \mathcal{S}$ . The output of the function  $\mathcal{F}$  represents the shortest displacement from the point  $q$  to the implicit surface, denoted as  $s(q) \in \mathcal{R}^3$ . In contrast to the completely implicit method, we introduce a geometric prior during the UDF prediction process, which will be explained in detail. Moving forward, we need to extract the surface from the function  $\mathcal{F}$ . This surface corresponds to the zero-level set of the displacement, defined as  $\mathcal{M} = \{q \mid \|s(q)\|_2 = 0, q \in \mathcal{S}\}$ .

*b) Explanation of Output:* According to the definition of  $s(q)$ , we can observe that  $\|s(q)\|_2$  represents the unsigned distance function (UDF) of the query point  $q$ . The reason why we do not directly predict the UDF of the query point is for the sake of convenience during training. Calculating

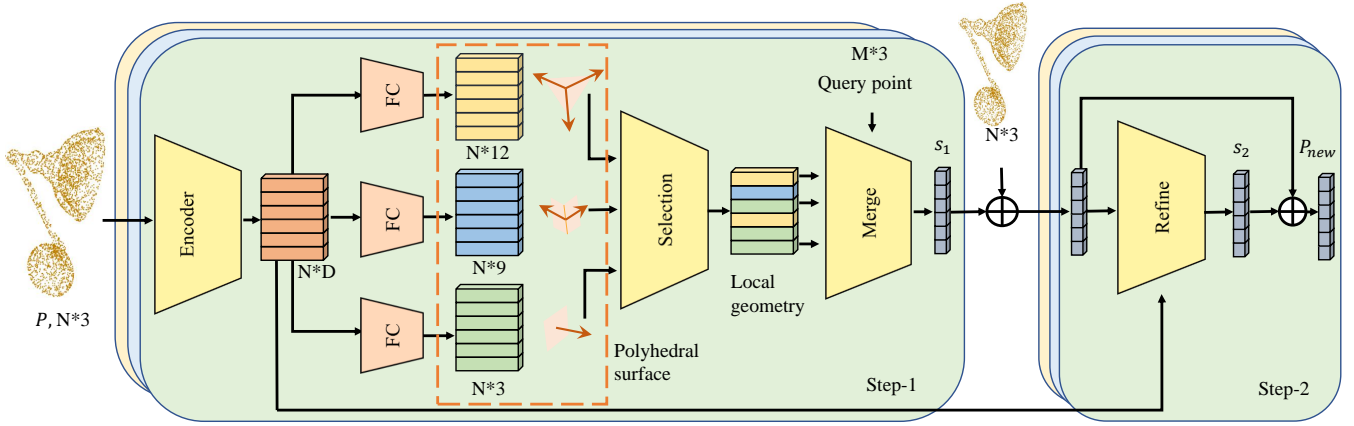


Fig. 3: The pipeline of the whole processing.

gradient from UDF field is time-consuming. Many point cloud reconstruction methods, such as [14], [12], [10], [24] require additional surface information as supervision, such as the SDF of the query point or determining whether two query points are on the same side of the surface. However, our method does not rely on any other supervision besides the input point cloud. This is because we can easily obtain a new point cloud using the function  $\mathcal{F}$ . Specifically, the new point cloud is obtained as  $\mathcal{P}_{new} = \{q + s(q) \mid q \in \mathcal{S}\}$ . By using the chamfer distance, we can encourage the two point clouds,  $\mathcal{P}_{new}$  and  $\mathcal{P}$ , to be close to each other. This approach is convenient during the training process because we can easily obtain a point cloud from  $s(q)$ . On the other hand, if the output of  $\mathcal{F}$  is the UDF of the query point, we will have to calculate the gradient of the query point to determine the displacement, which would be time-consuming.

*c) Architecture:* The main architecture is shown in Fig. 3. The backbone of the architecture, called encoder, consists of 4 layers of point cloud transformers [25] that extract per-point features from the point cloud. Each point  $p_i$  in the point cloud is assigned its per-point feature  $f_i$ . The next step is to predict the local geometry based on these features. If the local geometry is a plane, we predict the normal of the plane. If it is a polyhedral surface, we predict the corresponding normals. The selection of the local geometry type is based on the minimum average distance from the neighbor points to the surface of the local geometry. This approach increases the flexibility of the geometry prior compared to only considering planes as in SuperUDF [1]. Moreover, we do not require a local coordinate system.

After obtaining the per-point feature and parameter of local surface, we adopt a 2-steps way to calculate the displacement from query point to the implicit surface. In the first step, for every query point, we find the  $k_2$  nearest neighbors in the point cloud and calculate the displacement from the query point to each neighbor surface. These displacements are then averaged using weights generated by a learning-based weight generator. In the second step, we use a neural network to directly obtain a refined displacement from the shifted query point to the target surface. The two displacements are added together to obtain the final displacement. Through these two successive steps in

the decoder period, we can determine the displacement from any query point in space to the nearest surface.

The architecture is composed of the encoder backbone and the decoder part, which together form the function  $\mathcal{F}(\mathcal{P}, q)$ .

### B. plane

We propose three local geometries to enhance the flexibility of the local geometry prior when a local coordinate system is not available. The first one is a plane. On flat surface, plane is a good fitting for the local patch. To define a plane, we only need to estimate the normal vector and a center point. Specifically, given a point  $p_i$  in the point cloud, we use three fully connected layers (FC) to estimate the normal vector as follows:

$$\begin{aligned} n_i &= MLP_1(f_i) \\ n_i &= \frac{n_i}{\|n_i\|_2}, \end{aligned} \quad (1)$$

once the plane is defined, we can easily calculate the displacement from any query point  $q_j$  to the plane using the following equation:

$$s_{plane}(p_i, q_j) = \langle p_i - q_j, n_i \rangle n_i \quad (2)$$

Here,  $\langle \cdot, \cdot \rangle$  denotes the inner product.

### C. Dihedral surface

The dihedral surface is a versatile structure that can be used to fit various shapes, such as patches in tables, chairs and more. It offers an advantage over merging several planes as it allows for better preservation of sharp features on the turning surface, as depicted in Fig. 4. To describe the dihedral surface, we require two normals. Similar to planes, these normals are estimated from the feature of point  $p_i$  using a Multi-Layer Perceptron (MLP),

$$\begin{aligned} n_{i_1}, n_{i_2}, c_i &= MLP_2(f_i), \\ n_{i_1} &= \frac{n_{i_1}}{\|n_{i_1}\|_2}, \\ n_{i_2} &= \frac{n_{i_2}}{\|n_{i_2}\|_2}, \\ c_i &= Tanh(c_i) * 0.01 \end{aligned} \quad (3)$$

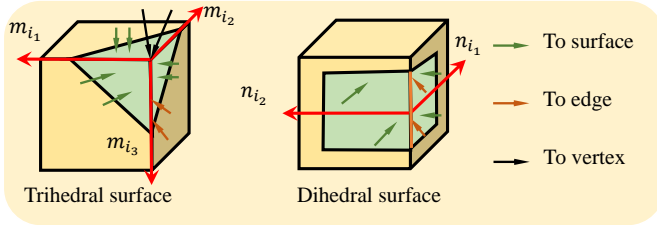


Fig. 4: The distance from query point to trihedral surface and dihedral surface.

where  $n_{i_1}$  and  $n_{i_2}$  are the normals,  $c_i$  is a local displacement which can move the dihedral surface. The reason why we need a local displacement is obvious.  $p_i$  might not be exactly on the edge of the turning surface and a local displacement can move the dihedral surface to the right position.

To calculate the distance from a query point  $q_j$  to the dihedral surface of  $p_i$ , we need to determine the closest point on the dihedral surface to  $q_j$ . This process is illustrated in Algorithm 1, and you can refer to Fig. 4 for a visual representation.

---

**Algorithm 1:** Calculate  $s_{dihedral}(p_i, q_j)$ 


---

**Input:**  $n_{i_1}, n_{i_2}, c_i, p_i, q_j$

**Output:**  $s_{dihedral}(p_i, q_j)$

- 1 initialization
  - 2  $s_{dihedral}(p_i, q_j) = \inf$
  - 3  $s_{i_1} = D(q_j, halfplane_{i_1})$  /\* the shortest displacement from  $q_j$  to half plane controlled by  $n_{i_1}$  \*/
  - 4  $s_{i_2} = D(q_j, halfplane_{i_2})$  /\* the shortest displacement from  $q_j$  to half plane controlled by  $n_{i_2}$  \*/
  - 5  $s_{dihedral}(p_i, q_j) = \min(s_{i_1}, s_{i_2})$  /\* min means vector with minimum  $L_2$  norm \*/
- 

#### D. Trihedral surface

We use three normals to represent the trihedral face, as depicted in Fig. 4. The trihedral surface can be used to represent the corners of a cube as well as the similarity of a cone. Similar to the dihedral surface, using the trihedral surface to represent corners or cones preserves sharp surfaces. The three normals of the trihedral surface are estimated from the feature  $f_i$  of point  $p_i$  using the following equations:

$$m_{i_1}, m_{i_2}, m_{i_3}, d_i = MLP_3(f_i), \quad (4)$$

$$m_{i_1} = m_{i_1} / \|m_{i_1}\|_2, \quad (5)$$

$$m_{i_2} = m_{i_2} / \|m_{i_2}\|_2, \quad (6)$$

$$m_{i_3} = m_{i_3} / \|m_{i_3}\|_2, \quad (7)$$

$$d_i = \text{Tanh}(d_i) * 0.01, \quad (8)$$

where  $m_{i_1}, m_{i_2}, m_{i_3}$  are the normals and  $d_i$  is the local displacement of the trihedral surface center.

To calculate the distance from query point  $q_j$  to the trihedral surface of  $p_i$ , we need to determine the closest point on the trihedral surface to  $q_j$ . This is illustrated in Algorithm 2, and you can refer to Fig. 4 for a visual representation.

---

**Algorithm 2:** Calculate  $s_{trihedral}(p_i, q_j)$ 


---

**Input:**  $n_{i_1}, n_{i_2}, c_i, p_i, q_j$

**Output:**  $s_{trihedral}(p_i, q_j)$

- 1 initialization
  - 2  $s_{trihedral}(p_i, q_j) = \inf$
  - 3  $s_{i_1} = D(q_j, halfplane_{i_1})$  /\* the shortest displacement from  $q_j$  to half plane controlled by  $m_{i_1}$  \*/
  - 4  $s_{i_2} = D(q_j, halfplane_{i_2})$  /\* the shortest displacement from  $q_j$  to half plane controlled by  $m_{i_2}$  \*/
  - 5  $s_{i_3} = D(q_j, halfplane_{i_3})$  /\* the shortest displacement from  $q_j$  to half plane controlled by  $m_{i_3}$  \*/
  - 6  $s_{trihedral}(p_i, q_j) = \min(s_{i_1}, s_{i_2}, s_{i_3})$  /\* min means vector with minimum  $L_2$  norm \*/
- 

#### E. Choose method

After constructing three local geometries, the next step is to determine which one to choose at point  $p_i$ . We have devised a simple yet effective method for this selection. The underlying principle is that if we have built a proper local geometry, all the neighbor points should lie exactly on the surface. To elaborate, given a point  $p_i$ , we select  $k_1$  neighboring points from the point cloud  $\mathcal{P}$ , denoted as  $\{p_{i_1}, \dots, p_{i_{k_1}}\}$ . We then calculate the average distance for each local geometry using the following formulas:

$$D_{plane_i} = \frac{1}{k_1} \sum_{l=0}^{k_1} s_{plane}(p_i, p_{i_l}) \quad (9)$$

$$D_{dihedral_i} = \frac{1}{k_1} \sum_{l=0}^{k_1} s_{dihedral}(p_i, p_{i_l}) \quad (10)$$

$$D_{trihedral_i} = \frac{1}{k_1} \sum_{l=0}^{k_1} s_{trihedral}(p_i, p_{i_l}) \quad (11)$$

$$D_i = \min(D_{plane_i}, D_{dihedral_i}, D_{trihedral_i}), \quad (12)$$

where  $\min()$  is a function that selects the vector with the minimum  $L_2$  norm. The local geometry that yields the minimum average distance, obtained by  $I_i = \text{argmin}(D_{plane_i}, D_{dihedral_i}, D_{trihedral_i})$ , is chosen as the final method.

#### F. Local Geometry Merge

Through the aforementioned pipeline, we are able to construct the local geometry for each point  $p_i$ . However, these individual local geometries need to be merged using adaptive weights. Instead of directly merging the local geometries, we calculate the average displacement for each

point. Specifically, for a query point  $q_j$ , we first identify its  $k_2$  neighboring points in  $\mathcal{P}$ , denoted as  $\{p_{j_1}, \dots, p_{j_{k_2}}\}$ . Each neighbor point has its own local geometry and corresponding displacement, defined as  $s_g(p_{j_l}, q_j) = (s_{plane}(p_{j_l}, q_j), s_{dihedral}(p_{j_l}, q_j), s_{triangular}(p_{j_l}, q_j)) [I_{j_l}]$ , where  $[I_{j_l}]$  means index. Then, the averaged displacement based on the local geometries is computed as follows:

$$s_g(q_j) = \sum_{l=0}^{k_2} w(p_{j_l}, q_j) \cdot s_g(p_{j_l}, q_j), \quad (13)$$

Here,  $w(p_{j_l}, q_j)$  represents the adaptive weight learned through a neural network.

Regarding the weight  $w(p_{j_l}, q_j)$ , we first predict a scale parameter for each point  $p_i$  based on its point feature  $f_i$  using a multi-layer perceptron (MLP) with four layers:

$$r_i = MLP_4(f_i). \quad (14)$$

Then, we consider the relative distance and the scale parameter together using the Softmax operator,

$$Softmax\left(-\frac{\|p_{j_1} - q_j\|_2}{\theta r_i}, \dots, -\frac{\|p_{j_{k_2}} - q_j\|_2}{\theta r_i}\right), \quad (15)$$

where  $\theta$  is a hyper-parameter.

### G. Displacement Refinement

After the initial data processing in the pipeline mentioned above, the query point is moved to the surface based on the local geometry. A simple neural network is then employed to further refine the displacement. Specifically, for the moved query point  $q_j + s_g(q_j)$ , the local geometry is encoded using positional encoding, followed by a multi-layer perceptron (MLP). This can be expressed as:

$$PE(q_j + s_g(q_j), p_i) = MLP_5(Positional(q_j + s_g(q_j) - p_i)), \quad (16)$$

Here, the function *Positional* represents positional encoding [26]. Subsequently, a point transformer [25] is utilized to obtain the feature of  $q_j$ , as shown in the following equation:

$$f_{q_j + s_g(q_j)} = \sum_{l=1}^{k_2} PointTrans(PE(q_j + s_g(q_j), p_{j_l}), f_{j_l}). \quad (17)$$

Finally, a MLP followed by a Tanh activation function is employed to predict the refined displacement:

$$s_{refined}(q_j + s_g(q_j)) = Tanh(MLP_6(f_{q_j + s_g(q_j)})). \quad (18)$$

Consequently, the total displacement is determined by the sum of the geometric displacement  $s_g(q_j)$  and the refined displacement  $s_{refined}(q_j + s_g(q_j))$ , represented as  $s(q_j) = s_g(q_j) + s_{refined}(q_j + s_g(q_j))$ .

### H. Losses

Our training procedure is self-supervised, with the only supervision being the input point cloud. In the training procedure, we introduce three separate losses. First, we aim for  $\mathcal{F}(\mathcal{P}, q)$  to accurately predict the displacement from any query point to the nearest surface. To achieve this, we sample a new point cloud,  $\mathcal{P}_{new}$ , from the function  $\mathcal{F}(\mathcal{P}, q)$ . The sampling method is straightforward. We randomly select  $m$  points around the original point cloud  $\mathcal{P}$  to obtain the query point set  $Q = q_1, \dots, q_m$ . Then, we calculate the displacement of each query point  $s(q_i)$ , where  $i \in \{1, \dots, m\}$ . Finally, the new point cloud set  $\mathcal{P}_{new}$  is defined as  $\{q_1 + s(q_1), \dots, q_m + s(q_m)\}$ . We measure the distance between  $\mathcal{P}$  and  $\mathcal{P}_{new}$  using chamfer distance, represented by the equation:

$$L_{CD_1} = \frac{1}{m} \sum_{j=1}^m \min_{i=1}^n \|q_j + s(q_j) - p_i\|_1. \quad (19)$$

To supervise the network in predicting reasonable parameters of local geometry, such as the normal of a plane and the normals of polyhedral surfaces, we propose a local displacement regularization term. The main idea is to minimize the displacement from query points to target surfaces. Specifically, for each point  $p_i$  in the point cloud, we find its  $k_1$ -nearest neighbors in the point cloud  $\mathcal{P}$ . These  $k_1$  neighbor points should lie on the local geometry of point  $p_i$ . The second loss is defined as:

$$L_{local} = \frac{1}{n} \sum_{i=1}^n D_i. \quad (20)$$

Third, we incorporate a UDF (Unsigned Distance Function) regularization term, as proposed in [1], to ensure a continuous UDF distribution. The main idea is simple: the UDF should decrease evenly with a gradient of 1 from the query point to the surface, and the gradient direction should not change. This can be deduced from the definition of the UDF. For a query point  $q$ , its UDF is  $\|s(q)\|_2$ . For any point  $\tilde{q}$  in the path from  $q$  to the surface, the displacement direction should be the same as that of  $q$ , and the UDF should decrease with a gradient of 1. Let  $\tilde{q} = q + (1 - \alpha)s(q)$ , where  $\alpha \in [0, 1]$ . The corresponding regularization term is given by:

$$L_{UDF} = \left\| \frac{s(\tilde{q})}{1 - \alpha} - s(q) \right\|_2. \quad (21)$$

## IV. EXPERIMENTS

In this section, we evaluate the performance of our method on the 3 datates, including ShapeNetCore [27], ABC [28] and ScanNet [29]. We first show quantitative and qualitative comparison with previous state-of-the-art methods. Next, we conduct comprehensive ablation studies and robust analysis. Quantatively, we choose  $CD_1$  to measure the completeness and accuracy of reconstructed mesh. In short, we show how

we make use of chamfer distance to constrain the training,  $CD_1$  equation is shown as the Eq.(22),

$$CD_1 = \frac{1}{2N_x} \sum_{i=1}^{N_x} \|\mathbf{x}_i - \mathcal{S}_y(\mathbf{x}_i)\|_1 + \frac{1}{2N_y} \sum_{i=1}^{N_y} \|\mathbf{y}_i - \mathcal{S}_x(\mathbf{y}_i)\|_1, \quad (22)$$

$\{\mathbf{x}_i, i = 0 \dots N_x\}$  is the points set sampled from ground-truth mesh.  $\{\mathbf{y}_i, i = 0 \dots N_y\}$  is the point set sampled from reconstructed mesh.  $\mathcal{S}_y(\mathbf{x}_i)$  means the nearest point to  $\mathbf{x}_i$  in reconstructed point set.  $\mathcal{S}_x(\mathbf{y}_i)$  means the nearest point to  $\mathbf{y}_i$  in ground-truth point set.  $\|\cdot\|_1$  means  $L1 - distance$ .

### A. Implementation Details

*a) Network architecture:* Our network backbone consists of four Point Transformer blocks, with the dimensions of 64, 128, 256, 256 respectively. We use  $k = 36$  nearest neighbor points as the local patch. After obtaining per-point feature, the network has two branches. In the first branch, we use the neighbor points of input point cloud to supervise the trihedral surface parameter, the number of neighbor points  $k_1$  is 36. In another branch, we predict  $r_i$  in Eq. (15) of every point. After merging the local polyhedral surface, we adopt a refinement layer implemented by point transformer, the k-nearest neighbor of the refinement step is 12 and the feature dimension is 64. Finally, we adopt a MLP to predict the 3-dimension refinement shift. During training, we adopt cosine learning rate adjustment [30], the initial learning rate is 0.001. We use Adam [31] optimizer to learn the parameter. The batch-size is 2. The query point number is 6000. The query point for training is obtained by randomly sampling point around the original point with the uniform distribution  $U(-0.03, 0.03)$ . During testing, to obtain the UDF in the whole space, we first partition the space into  $256^3$  voxels. We use the network to predict the UDF of the voxel center. Because our representation is not SDF, we do not use Marching Cube[32] to extract mesh. After obtaining the UDF of every voxel, we apply this [1] to extract the mesh.

### B. Shape Surface Reconstruction

In order to show the reconstruction performance of polyhedral surface, we first select a most widely-used dataset for point cloud reconstruction, ShapeNet. It contains 13 classes. For every class, we random select 100 shapes for test. Because the whole pipeline is self-supervised, we do not need to partition the train and test dataset. The result is shown in Tab. I. From the Tab. I, we can see that in most classes, our method outperform other method. Especially, we should focus on the comparison between ours and SuperUDF [1]. The most important difference between ours and SuperUDF [1] is the geometry prior. We use polyhedral surface while SuperUDF use a simple plane instead. Thus, from the comparison, we can see the improvement from the polyhedral surface. We can see that ours can outperform SuperUDF in most classes.

Class	GIFS [24]	CAP [3]	NPull [17]	SuperUDF [12]	Ours
airplane	0.0026	0.0031	0.0037	<b>0.0022</b>	0.0023
bench	0.0058	0.0059	0.0079	0.0029	<b>0.0027</b>
cabinet	0.0104	0.0048	0.0067	0.0039	<b>0.0036</b>
car	0.0052	0.0054	0.0060	0.0029	<b>0.0025</b>
chair	0.0041	0.0042	0.0122	0.0039	<b>0.0038</b>
display	0.0055	0.0047	0.0049	<b>0.0034</b>	0.0041
lamp	0.0078	0.0082	0.0089	0.0030	<b>0.0027</b>
speaker	0.0081	0.0063	0.0075	0.0041	<b>0.0038</b>
rifle	0.0029	0.0013	0.0016	0.0011	<b>0.0010</b>
sofa	0.0069	0.0050	0.0051	0.0033	<b>0.0030</b>
table	0.0065	0.0088	0.0117	0.0025	<b>0.0022</b>
phone	0.0049	0.0024	0.0028	0.0021	<b>0.0019</b>
vessel	0.0033	0.0025	0.0037	0.0021	<b>0.0021</b>
Mean	0.0057	0.0048	0.0063	0.0028	<b>0.0027</b>

TABLE I:  $CD_1$  comparison on ShapeNet within 13 classes

Method	SuperUDF [1]	CAP [3]	NPull [17]	GIFS [24]	Ours
$CD_1$	0.0063	0.0077	0.0092	0.0075	<b>0.0051</b>

TABLE II:  $CD_1$  comparison results on ABC 001 dataset.

Further more, we provide the visualization result for comparison as well. As shown in Fig. 5, we can see that ours can generate mesh faithful to the ground-truth.

Next, we show our result on ABC [28] 001. There are over 7000 shapes in ABC 001. Similar to ShapeNet, we randomly sample 100 shapes from it. The reason why we choose ABC is that shapes in ABC have lots of sharp feature. The result is shown in Tab. II. We can see that our method outperforms all other method. What's more, we provide the visualization result in Fig. 6. There is an important problem in UDF-based reconstruction. If UDF is not correct or noisy near the surface, the reconstructed mesh might have some holes. By comparing the ours and others, we can see that other methods have lots of holes except NPull [17], especially near the turning face and our method can generate mesh with less number of holes, while NPull is SDF-based method and has its own problem over-smooth. Because all the UDF-based methods mentioned above use the same mesh extraction method [1] and our method can generate the mesh with the least number of holes, polyhedral surface can improve the UDF quality especially near the turning surface.

### C. Scene Surface Reconstruction

In order to show the performance on open surface, we select the partially scanned scene, ScanNet [29]. First, we provide the quantitative result in Tab. III. We can see that our method can outperform other methods. What's more, we provide the visualization result on final mesh in Fig. 7. Comparing with SuperUDF [1], our method can generate boundary faithful to the GT, while the boundary of SuperUDF expands outward a lot. This is for the reason that the local geometry prior plane near the boundary will expand and cannot fit the local half plane. However, our polyhedral surface can fit the half plane thus can generate better boundary.

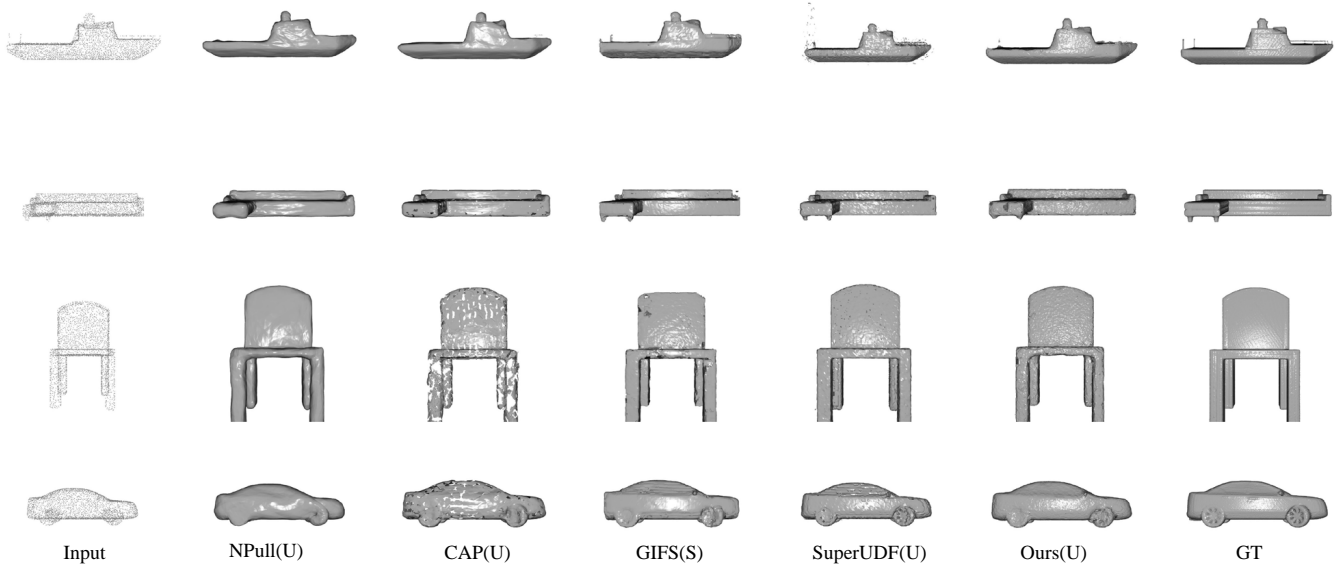


Fig. 5: Visualized results of our method and state-of-the-art alternatives on ShapeNet. (S) mean supervised method and (U) means unsupervised method. Methods are NPull[17], CAP[3], GIFS[24], SuperUDF[1] and Ours. The number of input point cloud is 3000.

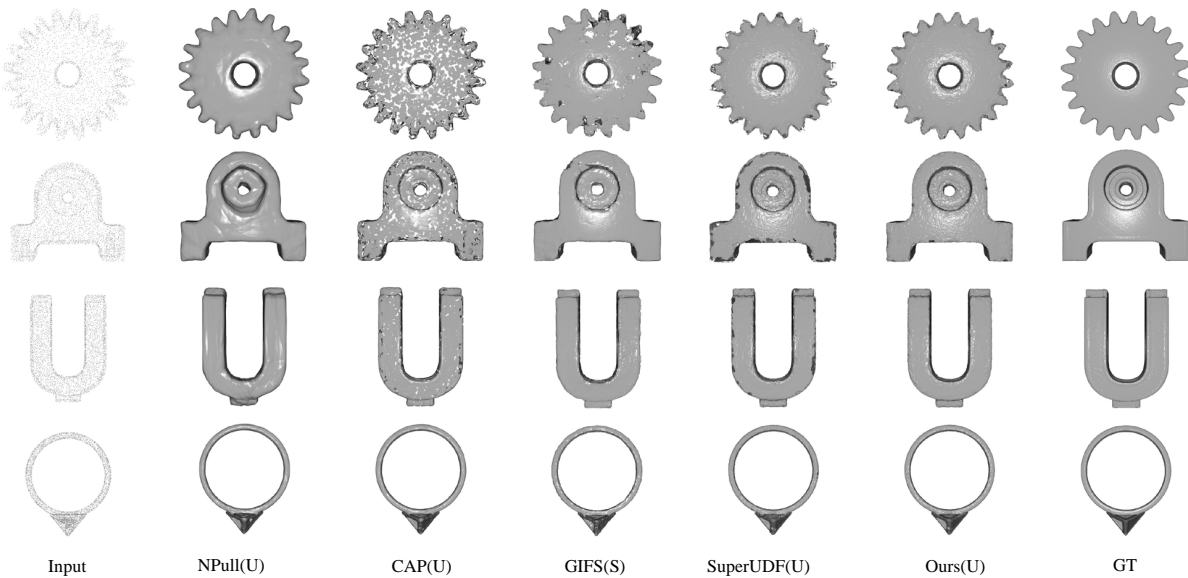


Fig. 6: Visualized results of our method and state-of-the-art alternatives on ABC 001. (S) mean supervised method and (U) means unsupervised method. Methods are NPull[17], CAP[3], GIFS[24], SuperUDF[1] and Ours. The number of input point cloud is 3000.

Method	SuperUDF [1]	CAP [3]	GIFS [24]	Ours
$CD_1$	0.0039	0.0044	0.0043	<b>0.0033</b>

TABLE III:  $CD_1$  comparison on ScanNet with the number of sample point 10000.

dataset	Plane	dihedral	trihedral	Plane+dihedral+trihedral
ABC	0.0063	0.0085	0.0078	<b>0.0051</b>
ScanNet	0.0039	0.0057	0.0046	<b>0.0033</b>

TABLE IV: Ablation study of polyhedral surface.

#### D. Ablation Study

The key contribution of this paper is the polyhedral surface, including dihedral and trihedral surface as the geometry prior. Therefore, we want to show how much contribution every part makes. In total, we design 4 experiments. In detail,

we show the result under different compositions of the 3 geometry prior in Tab. IV. We are not surprised to see that plane+dihedral+trihedral achieves best result. However, how much the 3 geometry priors contributes separately is still a problem. Thus, we provide the visualization result to obtain

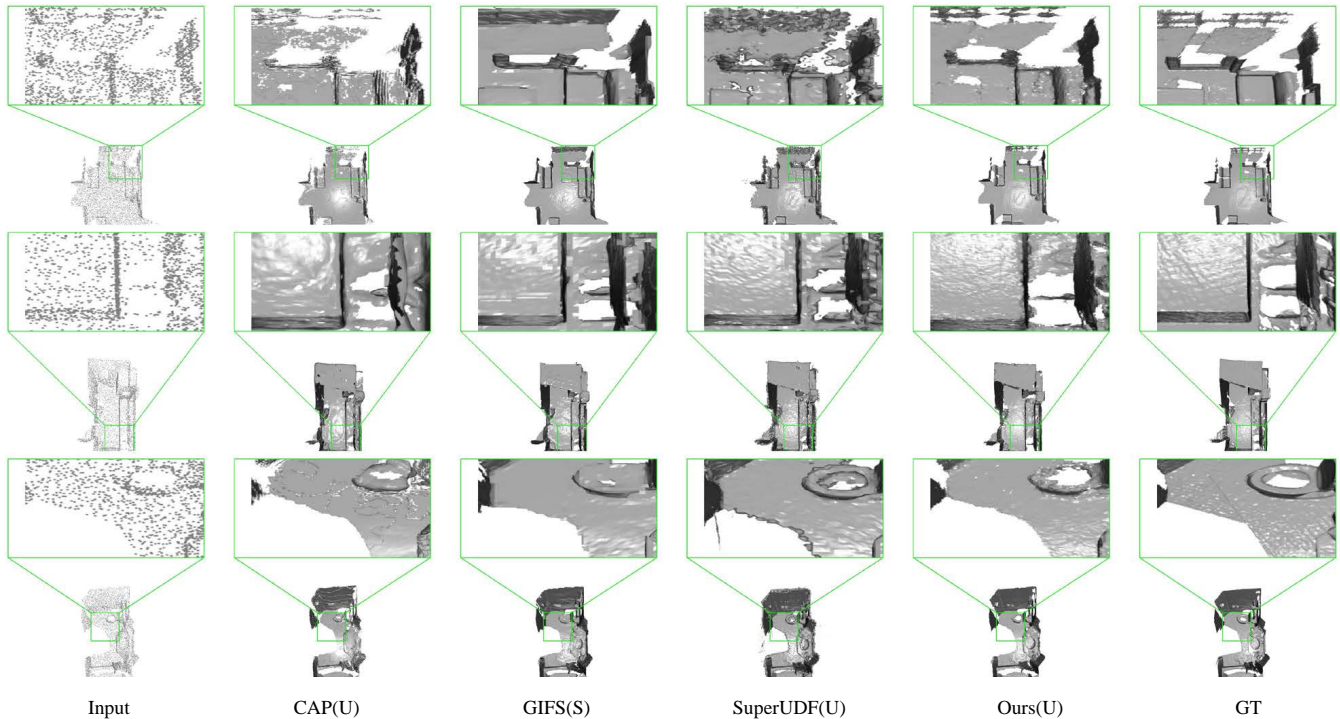


Fig. 7: Visualized results of our method and state-of-the-art alternatives on ScanNet. (S) mean supervised method and (U) means unsupervised method. Methods are CAP[3], GIFS[24], SuperUDF[1] and Ours. The number of input point cloud is 10000.

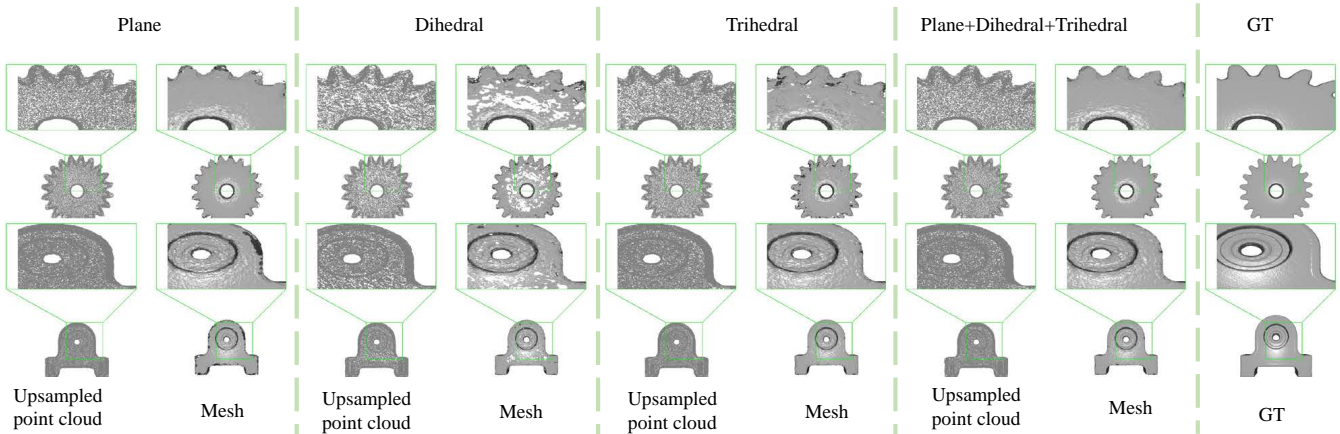


Fig. 8: Evaluation of the effectiveness of the polyhedral surface on flat surface and turning surface.

a deeper sight in Fig. 8 and Fig. 9. First, we focus on the sharp feature problem in Fig. 8, we can see that dihedral surface and trihedral surface cannot work well independently and will lead to some holes on the flat surface due to its flexibility. Plane itself can generate rather good result on the flat surface. However, in sharp turning surface and boundary surface, it produces unsatisfactory result. The combination of the 3 geometry prior can produce best result. Next, we focus on the boundary problem in Fig. 9, we can see that the method with only plane will expand outward near the boundary for the reason that the geometry prior plane cannot fit the the half plane near the boundary. From the ablation study, we can conclude that polyhedral surface have priority

on representation of turning surface and boundary surface.

### E. Robust Analysis

In this part, we provide the analysis of the important hyper-parameters. First we analyze the robustness of the  $k_1$  in Tab. V. We can see that when  $k_1$  is 36, the performance reaches the peak. Meanwhile, when  $k_1$  varies in [12, 24, 36, 48], the performance is relatively robust.

Next, we provide the analysis of the parameter in merging the local surface,  $\theta$  in Tab. VI. We can see that when  $\theta$  varies in [50, 100, 200, 400], the performance varies a little. When  $\theta$  is 100, the performance reaches the peak.

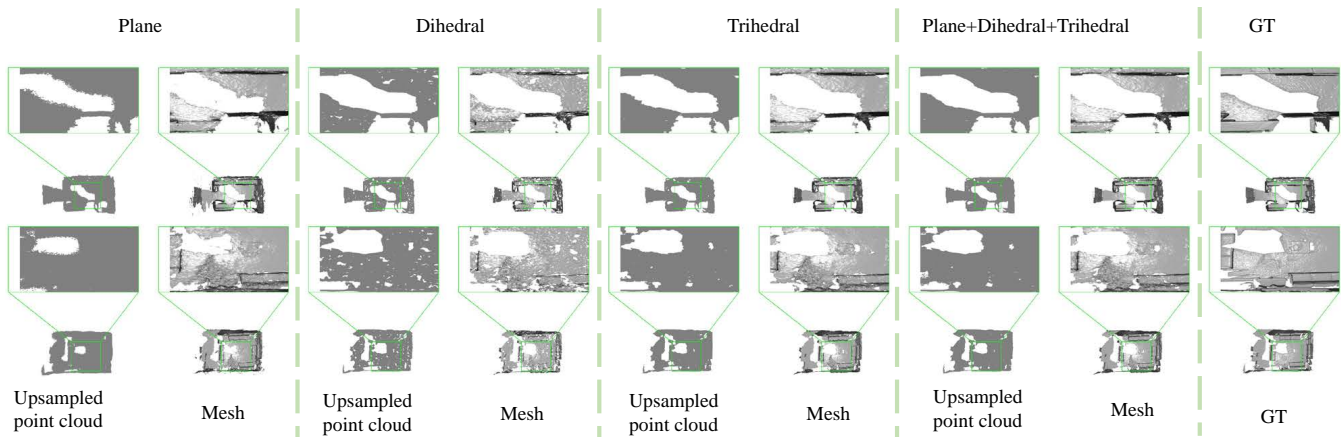


Fig. 9: Evaluation of the effectiveness of polyhedral surface on the boundary of open surface.

$k_1$	12	24	36	48
$CD_1$	0.0056	0.0053	<b>0.0051</b>	0.0.0052

TABLE V: The robust analysis of  $k_1$  on ABC 001.

$\theta$	50	100	200	400
$CD_1$	0.0053	0.0051	0.0052	0.0054

TABLE VI: The robust analysis of  $\theta$  on ABC 001

### F. Efficiency Analysis

We only add polyhedral surface comparing with SuperUDF[1]. Obviously, the representation is more complex than plane. In this part, we provide the time comparison between plane representation and polyhedral surface representation during training and testing part in Tab VII. We can see that although polyhedral surface is more complex, the time cost during training and testing do not increase much. This is for the reason that the complexity increased by the polyhedral surface is too low in modern computer.

In Tab. VIII, we can see the FLOP and the number of parameters comparison. We can see that although FLOP and the number of parameters of polyhedral surface is more than plane, they are both very small. Here, we only calculate the memory and FLOP of geometry priors prediction part and cut down the calculation cost of backbone network.

## V. CONCLUSION

We propose polyhedral surface to represent local surface, including dihedral surface and trihedral surface. It can preserve local sharp feature of turning surface, corner of cube and boundary surface. The polyhedral surface only relies on

Method	NPull	CAP	SuperUDF	Ours
distance prediction	29min22s	21min56s	9s	10s

TABLE VII: Time Efficiency comparison between ours and other method of (signed or unsigned) distance prediction.

Method	SuperUDF	plane+dihedral+trihedral
#parameter(MB)	0.126	0.230
#FLOP(G)	8.097	10.271

TABLE VIII: The number of parameter and FLOP of the polyhedral surface. The number of point cloud is 3000 and the number of query point is 6000

normal instead of a local coordinate system. Thus, we can avoid the coordinate consistency problem. In experiments, our method achieves comparable results with little computation cost. However, there is still some problems of the representation. For example, it cannot handle noisy input for the reason of local view. It is hard to seek a balance between the sharp feature and noisy influence. This problem can be the future work.

## REFERENCES

- [1] Y. S. Hui Tian, Chenyang Zhu and K. Xu, “Superudf: Self-supervised udf estimation for surface reconstruction,” <https://arxiv.org/abs/2308.14371>, 2023.
- [2] J. Park, P. Florence, J. Straub, R. Newcombe, and S. Lovegrove, “DeepSDF: Learning continuous signed distance functions for shape representation,” in *2019 IEEE/CVF Conference on Computer Vision and Pattern Recognition (CVPR)*, 2019.
- [3] J. Zhou, B. Ma, L. Yu-Shen, F. Yi, and H. Zhizhong, “Learning consistency-aware unsigned distance functions progressively from raw point clouds,” in *Advances in Neural Information Processing Systems (NeurIPS)*, 2022.
- [4] M. Atzmon and Y. Lipman, “SAL: Sign Agnostic Learning of Shapes From Raw Data,” in *2020 IEEE/CVF Conference on Computer Vision and Pattern Recognition (CVPR)*. Seattle, WA, USA: IEEE, Jun. 2020, pp. 2562–2571.
- [5] —, “SALD: Sign Agnostic Learning with Derivatives,” Oct. 2020.
- [6] R. Venkatesh, S. Sharma, A. Ghosh, L. Jeni, and M. Singh, “DUDE: Deep Unsigned Distance Embeddings for Hi-Fidelity Representation of Complex 3D Surfaces,” Dec. 2020.
- [7] J. P. Richa, J.-E. Deschaut, F. Goulette, and N. Dalmaso, “UWED: Unsigned Distance Field for Accurate 3D Scene Representation and Completion,” p. 20.
- [8] T. Li, X. Wen, Y. S. Liu, H. Su, and Z. Han, “Surface reconstruction from point clouds by learning predictive context priors,” in *Proceedings of the IEEE/CVF Conference on Computer Vision and Pattern Recognition*, 2022.
- [9] X. T. Peng-Shuai Wang, Yang Liu, “Dual octree graph networks for learning adaptive volumetric shape representations,” in *ACM Transactions on Graphics*, 2022.
- [10] S.-L. Liu, H.-X. Guo, H. Pan, P.-S. Wang, X. Tong, and Y. Liu, “Deep implicit moving least-squares functions for 3d reconstruction,” in *Proceedings of the IEEE/CVF Conference on Computer Vision and Pattern Recognition*, 2021, pp. 1788–1797.
- [11] L. Mescheder, M. Oechsle, M. Niemeyer, S. Nowozin, and A. Geiger, “Occupancy networks: Learning 3d reconstruction in function space,” in *2019 IEEE/CVF Conference on Computer Vision and Pattern Recognition (CVPR)*, 2019.
- [12] S. Peng, M. Niemeyer, L. Mescheder, M. Pollefeys, and A. Geiger, *Convolutional Occupancy Networks*, 2020.
- [13] Z. Mi, Y. Luo, and W. Tao, “Ssrnet: Scalable 3d surface reconstruction network,” in *2020 IEEE/CVF Conference on Computer Vision and Pattern Recognition (CVPR)*, 2020.
- [14] A. Boulch and R. Marlet, “Poco: Point convolution for surface reconstruction,” in *Proceedings of the IEEE/CVF Conference on Computer Vision and Pattern Recognition*, 2022.
- [15] P. Erler, P. Guerrero, S. Ohrhallinger, M. Wimmer, and N. J. Mitra, “Points2surf: Learning implicit surfaces from point cloud patches,” 2020.
- [16] J. Chibane, A. Mir, and G. Pons-Moll, “Neural unsigned distance fields for implicit function learning,” 2020.
- [17] B. Ma, Z. Han, Y. S. Liu, and M. Zwicker, “Neural-pull: Learning signed distance functions from point clouds by learning to pull space onto surfaces,” 2020.
- [18] B. Ma, Y.-S. Liu, and Z. Han, “Reconstructing Surfaces for Sparse Point Clouds With On-Surface Priors,” in *2022 IEEE/CVF Conference on Computer Vision and Pattern Recognition*, p. 11.
- [19] T. Li, X. Wen, Y. S. Liu, H. Su, and Z. Han, “Learning deep implicit functions for 3d shapes with dynamic code clouds,” in *Proceedings of the IEEE/CVF Conference on Computer Vision and Pattern Recognition*, 2022.
- [20] B. Guillard, F. Stella, and P. Fua, “Meshudf: Fast and differentiable meshing of unsigned distance field networks,” *arXiv e-prints*, 2021.
- [21] Alexa, M., Behr, J., Cohen-Or, D., Fleishman, S., Levin, and Silva, “Computing and rendering point set surfaces,” *Visualization and Computer Graphics, IEEE Transactions on*, 2003.
- [22] R. Kolluri, “Provably good moving least squares,” *ACM Transactions on Algorithms (TALG)*, vol. 4, no. 2, pp. 1–25, 2008.
- [23] S. Fleishman, D. Cohen-Or, and C. T. Silva, “Robust moving least-squares fitting with sharp features,” *Acm Trans Graph*, vol. 24, no. 3, pp. 544–552, 2005.
- [24] J. Ye, Y. Chen, N. Wang, and X. Wang, “GIFS: Neural Implicit Function for General Shape Representation,” in *Proceedings of the IEEE/CVF Conference on Computer Vision and Pattern Recognition*, 2022, p. 11.
- [25] H. Zhao, L. Jiang, J. Jia, P. H. Torr, and V. Koltun, “Point transformer,” in *Proceedings of the IEEE/CVF International Conference on Computer Vision*, 2021, pp. 16 259–16 268.
- [26] M. Tancik, P. P. Srinivasan, B. Mildenhall, S. Fridovich-Keil, N. Raghuvan, U. Singhal, R. Ramamoorthi, J. T. Barron, and R. Ng, “Fourier features let networks learn high frequency functions in low dimensional domains,” 2020.
- [27] A. X. Chang, T. Funkhouser, L. Guibas, P. Hanrahan, Q. Huang, Z. Li, S. Savarese, M. Savva, S. Song, H. Su *et al.*, “Shapenet: An information-rich 3d model repository,” *arXiv preprint arXiv:1512.03012*, 2015.
- [28] S. Koch, A. Matveev, Z. Jiang, F. Williams, A. Artemov, E. Burnaev, M. Alexa, D. Zorin, and D. Panozzo, “Abc: A big cad model dataset for geometric deep learning,” in *The IEEE Conference on Computer Vision and Pattern Recognition (CVPR)*, June 2019.
- [29] A. Dai, A. X. Chang, M. Savva, M. Halber, T. Funkhouser, and M. Nießner, “ScanNet: Richly-annotated 3d reconstructions of indoor scenes,” in *Proc. Computer Vision and Pattern Recognition (CVPR), IEEE*, 2017.
- [30] I. Loshchilov and F. Hutter, “Sgdr: Stochastic gradient descent with restarts,” 2016.
- [31] D. P. Kingma and J. Ba, “Adam: A method for stochastic optimization,” *arXiv preprint arXiv:1412.6980*, 2014.
- [32] W. E. Lorensen and H. E. Cline, “Marching cubes: A high resolution 3d surface construction algorithm,” *ACM siggraph computer graphics*, vol. 21, no. 4, pp. 163–169, 1987.